MATERIALS SCIENCE

Networks with controlled chirality via self-assembly of chiral triblock terpolymers

Hsiao-Fang Wang[1], Po-Ting Chiu[1], Chih-Ying Yang[2], Zhi-Hong Xie[2], Yu-Chueh Hung[2], Jing-Yu Lee[3], Jing-Cherng Tsai[3], Ishan Prasad[4], Hiroshi Jinnai[5], Edwin L. Thomas[6], Rong-Ming Ho[1]*

Nanonetwork-structured materials can be found in nature and synthetic materials. A double gyroid (DG) with a pair of chiral networks but opposite chirality can be formed from the self-assembly of diblock copolymers. For triblock terpolymers, an alternating gyroid (G^A) with two chiral networks from distinct end blocks can be formed; however, the network chirality could be positive or negative arbitrarily, giving an achiral phase. Here, by taking advantage of chirality transfer at different length scales, G^A with controlled chirality can be achieved through the self-assembly of a chiral triblock terpolymer. With the homochiral evolution from monomer to multichain domain morphology through self-assembly, the triblock terpolymer composed of a chiral end block with a single-handed helical polymer chain gives the chiral network from the chiral end block having a particular handed network. Our real-space analyses reveal the preferred chiral sense of the network in the G^A, leading to a chiral phase.

INTRODUCTION

The basic shape of a gyroid network element [a single gyroid (SG)] is a threefold junction of three struts (i.e., trigonal planar) in which each strut connects to another trigonal planar each of which is rotated to form a three-dimensional (3D) network (*1*). By joining the nodes of the SG to create a periodic graph, one could readily identify helical paths along various screw axes of the SG. Chiral metamaterials constructed from chiral constituents, in which the nonzero dimensionless chirality parameter (κ) gives rise to a negative refractive index, are of great interest for applications such as the superlens to overcome the diffraction limit in imaging (*2*–*4*) and the materials with giant optical activity to enable previously unidentified optical effects (*5*). Moreover, it is believed that circular dichroism effect due to chirality may relate to insect communication (*6*). By using a SG network with controlled chirality as an optical device, it is feasible to separate right- and left-handed circularly polarized light (CPL), giving a circularly polarized beam splitter (i.e., chiral beam splitter) with different critical reflection angles for right- and left-handed CPL (*7*). Moreover, a SG network with controlled chirality has recently been demonstrated to give unique optical properties as chiral plasmonic metamaterials (*8*–*10*).

Most fabrication approaches for metamaterials today rely on top-down approaches. Yet, there is limitation on the overall size of the nanostructured materials produced from top-down methods, and the process is time-consuming. By contrast, self-assembly has emerged as a useful design approach to create well-ordered nanoscale structures. On the basis of thermodynamic consideration for stable equilibrium state, a double gyroid (DG) composed of a pair of continuous, interpenetrating but independent, coherent SG networks (one positive chirality and one negative chirality) in a matrix can be formed from the self-assembly of AB diblock copolymers to give an achiral cubic phase. The self-assembled DG is formed in synthetic and natural materials such as block copolymers (BCPs) (*11*–*13*), liquid crystals (*14*, *15*), lipids (*1*), surfactants (*15*, *16*), and biological assemblies (*17*, *18*). To achieve a particular handed SG network, chiral symmetry breaking is commonly observed in biological materials, for example, at the macroscopic size of a butterfly wing (*17*, *19*). Self-assembled achiral ABC triblock terpolymers (*20*, *21*) exhibit two compositionally distinct SGs networks to give an alternating gyroid (G^A) (*20*). Yet, the SG networks in each grain of the structure can arbitrarily exhibit either positive or negative chirality. The critical challenge for chiral network with controlled chirality from self-assembly thus remains and limits this approach for applications in chiral metamaterials owing to the inability to create a single chirality for a given network-forming component. Note that, by using a chiral monomer, a novel helical phase (H*) could be obtained in AB diblock copolymer composed of chiral block (designated as chiral block copolymer, BCP*) (*22*–*24*). Chirality transfers from molecular (monomeric) to conformational (chain) and, ultimately, to hierarchical (multichain domain) chirality in self-assembled BCPs* could be achieved to give the H* with controlled chirality, demonstrating the generic behaviors of homochiral evolution at different length scales from self-assembly (*25*–*27*).

To access the network with controlled chirality, chiral triblock terpolymers composed of an enantiomeric chiral end block, polyisoprene-*b*-polystyrene-*b*-poly(D-lactide) (PI-*b*-PS-*b*-PDLA), and polyisoprene-*b*-polystyrene-*b*-poly(L-lactide) (PI-*b*-PS-*b*-PLLA) were synthesized for self-assembly to scrutinize the chirality effects on triblock terpolymer self-assembly and the corresponding chirality transfer at different length scales. By carefully choosing the composition of each block, such that the PS is the matrix component and the polylactide block and the PI block are the dispersive components, to assure that the PLLA and PDLA blocks will form their own multichain domain network and if monomeric chirality transfer occurs, it is expected that each will form a left (PLLA) or a right (PDLA) network in every grain of the respective material.

RESULTS

Figure 1A shows the 1D small-angle x-ray scattering (SAXS) profile of the PI-*b*-PS-*b*-PLLA at which two reflections in the low-*q* region

[1]Department of Chemical Engineering, National Tsing Hua University, No. 101, Section 2, Kuang-Fu Road, Hsinchu, Taiwan 30013, R.O.C. [2]Institute of Photonics Technologies, National Tsing Hua University, No. 101, Section 2, Kuang-Fu Road, Hsinchu, Taiwan 30013, R.O.C. [3]Department of Chemical Engineering, National Chung Cheng University, No.168, Sec. 1, University Rd., Minhsiung, Chia-Yi, Taiwan 62142, R.O.C. [4]Department of Polymer Science and Engineering, University of Massachusetts, 120 Governors Drive, Amherst, MA 01003, USA. [5]Institute of Multidisciplinary Research for Advanced Materials, Tohoku University, 2-1-1, Katahira, Aoba-ku, Sendai 980-8577, Japan. [6]Department of Materials Science and NanoEngineering, Rice University, 6100 Main St., Houston, TX 77005, USA.
*Corresponding author. Email: rmho@mx.nthu.edu.tw

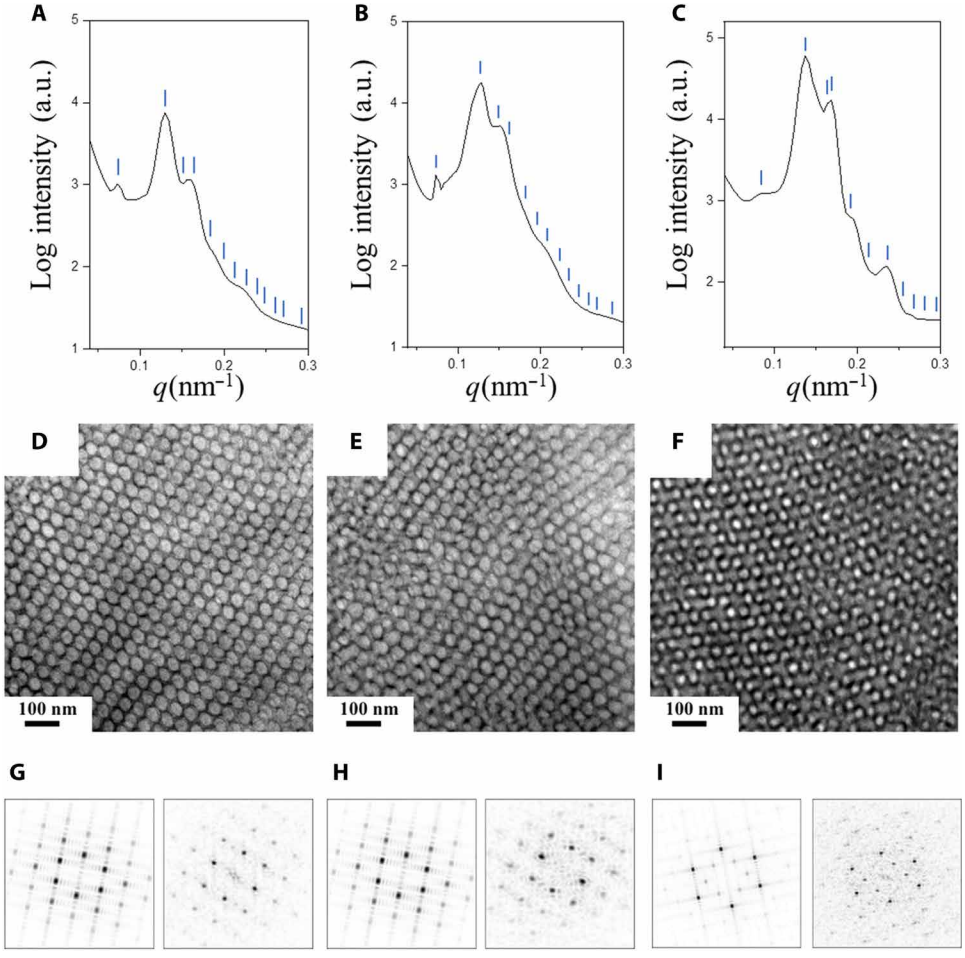

Fig. 1. Examination of self-assembled polylactide-based triblock terpolymers. (**A** to **C**) 1D small-angle x-ray scattering (SAXS) profiles, (**D** to **F**) OsO_4-stained TEM micrographs with viewing along [111], and (**G** to **I**) simulated (left) and experimental (right) FFT results of PI-*b*-PS-*b*-PLLA, PI-*b*-PS-*b*-PDLA, and PI-*b*-PS-*b*-PLA, respectively. The line symbols in the SAXS profiles indicate the predicted reflections with the relative *q* values of √2: √6: √8: √10: √12: √14: √16: √18: √20: √22: √24: √26: √30: √32 for the G^A structure (A and B) and√3: √8: √11: √12: √16: √19: √24: √27: √32: √35 for the D^A structure (C). The corresponding FFT results were acquired from the monograin region of the TEM micrographs. a.u., arbitrary units.

at the relative *q* value of √2: √6 can be found. By considering the large electron density contrast between the PLLA (ρ_L = 0.383 e/Å^3) with a volume fraction of 0.5 relative to the PS (ρ_S = 0.332 e/Å^3) and the PI (ρ_I = 0.312 e/Å^3) domains, we speculate that the reflections are attributed to the results from PLLA SG network structure having a space group of $I4_132$ (see the Supplementary Materials for details on the SAXS results of suggested PLLA gyroid). These two reflections were thus indexed as reflections from the (110) and (211) planes of the PLLA SG. The third broad peak was suggested to be a combination of the (220) and (310) reflections at the relative *q* value of √8: √10 from the PLLA SG structure. The lower degree of order for the self-assembled polylactide-based triblock terpolymers might be attributed to the effect of molecular weight on self-assembly. As reported by Epps and Bates (*28*), increasing the total molecular weight of the triblock might lead to the disruption of long-range order for the self-assembled triblock terpolymers. Similar results were also found in the PI-*b*-PS-*b*-PDLA (Fig. 1B). To unambiguously determine the self-assembled phase, it is necessary to combine the experimental results from the reciprocal-space imaging from SAXS and the real-space imaging from electron microscopy the phase identification. Figure 1 (D and E) shows representative transmission electron microscopy (TEM) 2D projections of the self-assembled PI-*b*-PS-*b*-PLLA and the PI-*b*-PS-*b*-PDLA samples, respectively. The OsO_4-stained PI microdomains appear dark whereas PS and polylactide microdomains appear bright, suggesting a (111) projection along the [111] direction of a PI gyroid; the corresponding fast Fourier transform (FFT) results are in line with the simulation (Fig. 1, G and H). Moreover, other images of the PI gyroid projected along different directions could be clearly observed (fig. S1). The combined scattering and imaging results thus suggest the formation of a G^A composed of a pair of gyroid networks (a polylactide gyroid and a PI gyroid) in a PS matrix.

In contrast to the chiral triblock terpolymers with G^A (which is a chiral ordered phase with threefold junction network), the 1D SAXS profile of polyisoprene-*b*-polystyrene-*b*-poly(D,L-lactide) (PI-*b*-PS-*b*-PLA) (an achiral triblock terpolymer) shows two reflections in the low-*q* region at the relative *q* values of √3: √8. With the similar experimental conditions to the G^A examined above, we speculate that the reflections should correspond to reflections from the (111) and (220) planes of a PLA single diamond (SD) network structure

having a space group of $Fd\bar{3}m$ in self-assembled PI-*b*-PS-*b*-PLA (Fig. 1C). The third board peak is a combination of the (311) and (222) reflections at the relative *q* value of √11: √12 from the PLA SD structure. The corresponding TEM projections and FFT results of the self-assembled phase of the PI-*b*-PS-*b*-PLA with OsO_4 staining, as shown in Fig. 1 (F and I) for the (111) projection and fig. S1 for other projections, evidence the formation of a PI diamond. The scattering and imaging results thus suggest the formation of an alternating diamond (D^A) (which is an achiral ordered phase with fourfold junction network). Accordingly, the chirality effects on the self-assembly of triblock terpolymers give rise to the formation of G^A with two chiral networks whereas the one without chiral end block results in the formation of D^A without chiral network. Figure S2 shows the comparison of the 1D SAXS profiles of PI-*b*-PS-*b*-PLLA, PI-*b*-PS-*b*-PDLA, and PI-*b*-PS-*b*-PLA to demonstrate the differences between G^A and D^A; as observed, the discrepancies can be identified. Note that G^A and D^A are expected in the phase diagram of achiral triblock terpolymers (*20*, *29*). For the polylactide-based triblock terpolymers synthesized in this study, as shown in Table 1, the number average molecular weights for PI-*b*-PS-*b*-PLLA, PI-*b*-PS-*b*-PDLA, and PI-*b*-PS-*b*-PLA are 41,300, 44,600, and 42,900 g/mol, respectively. The volume fractions for the PI, PS, and polylactide are quite asymmetric. In particular, the volume fraction for the PS matrix is approximately 0.35, while the one for the dispersed polylactide is approximately 0.5, which is much larger than the PS and the PI (0.15); this large asymmetry in constituted compositions, particularly with the large chiral end block, might be essential to control the chirality of the chiral end block gyroid.

Considering the chirality transfer from molecular to hierarchical chirality, intuitively, the formation of a gyroid with exclusive handedness can be achieved through homochiral evolution from self-assembly. Figure S3A shows the electronic circular dichroism (ECD) and corresponding absorption spectra of the PI-*b*-PS-*b*-PLLA, the PI-*b*-PS-*b*-PDLA, and the PI-*b*-PS-*b*-PLA in acetonitrile (AcCN) solution. A positive ECD signal from the PI-*b*-PS-*b*-PLLA and a negative one from the PI-*b*-PS-*b*-PDLA at 220 nm can be identified, attributed to the $n \rightarrow \pi^*$ transition of carboxylate chromophore in lactide, whereas the solution of the PI-*b*-PS-*b*-PLA yields no ECD signal. Having confirmed the molecular chirality in the backbone of the chain, vibration circular dichroism (VCD) was used to test whether the chirality transfer from molecule to conformation occurs to give a helical chain with specific handedness due to intrachain chiral interactions (*30*, *31*). The VCD and corresponding absorption spectra of the PI-*b*-PS-*b*-PLLA, the PI-*b*-PS-*b*-PDLA, and the PI-*b*-PS-*b*-PLA were measured by dissolving the samples in dichloromethane (CH_2Cl_2) solution (fig. S3B). For PI-*b*-PS-*b*-PLLA, owing to the C═O stretching motion of the carbonyl group in polylactide, a split-type Cotton effect with a positive one at 1767 cm^{-1} and a negative VCD band at 1753 cm^{-1} can be found. Consistently, a mirror image of the PI-*b*-PS-*b*-PLLA in the VCD spectrum of the PI-*b*-PS-*b*-PDLA can be clearly identified, and the PI-*b*-PS-*b*-PLA solution yields no VCD signal. Accordingly, on the basis of the coupled oscillator model (*32*), the helical PLLA and PDLA chains are left- and right-handed, respectively, in accordance with the signatures of the split-type Cotton effect in the VCD spectra (*25*); namely, the enantiomeric polymer chain has single-handed helicity. To investigate the suggested homochiral evolution from conformational to hierarchical chirality, solid-film samples of the self-assembled PI-*b*-PS-*b*-PLLA, PI-*b*-PS-*b*-PDLA, and PI-*b*-PS-*b*-PLA were prepared for spectroscopic examination. Similar to the results in the solution state, the opposite Cotton effects in the ECD spectra (fig. S3C) and the opposite split-type Cotton effects in the VCD spectra (fig. S3D) can be found from the solid films of PI-*b*-PS-*b*-PLLA and PI-*b*-PS-*b*-PDLA, and no ECD and VCD signals in the solid film of PI-*b*-PS-*b*-PLA. Those results suggest that the self-assembled phases will be constructed from preferred one-handed helical chain conformation in polylactide-based chiral triblock terpolymers (i.e., PI-*b*-PS-*b*-PLLA and PI-*b*-PS-*b*-PDLA) whereas the one from the PI-*b*-PS-*b*-PLA is built in by achiral polymer chains. By taking advantage of interchain chiral interactions, it is expected to form polylactide gyroid with controlled chirality. Obviously, the identification of chirality for the forming gyroid is essential. However, the chirality of gyroid from self-assembly is difficult to directly determine from conventional TEM images (2D projections) owing to the complicated morphology for the projection of network phase. Instead, electron tomography (3D TEM) can be used to visualize real-space morphologies by tomographic technology. Figure 2A shows the simulated image of PI gyroid with right-handed helical path along the [110] direction. The 3D reconstruction image–stained PI microdomain of the PI-*b*-PS-*b*-PLLA along the [110] direction (Fig. 2D) is exactly in line with the simulation results at which the right-handed helical path for the PI gyroid with threefold junctions could be clearly identified along the [110] direction. On the basis of the polymer chain sequences in the triblocks, the forming G^A should be composed of a pair of gyroid networks (a right-handed PI gyroid and a left handed PLLA gyroid) with the PS serving as a matrix as identified above. Consistently, the left-handed helical path for the PI gyroid network in the PI-PS-PDLA along the [110] direction could also be identified (Fig. 2E), similar to the simulation (Fig. 2B). By contrast, the reconstruction results suggest the formation of an achiral PI diamond with tetrapod network in the PI-*b*-PS-*b*-PLA (see the simulated and reconstruction results in Fig. 2, C and F, respectively).

To further examine the suggested G^A, templated electroless plating was carried out by performing hydrolysis on the polylactide-based triblock terpolymer to create a template for the synthesis of a SG

Table 1. Characterization of polylactide-based triblock terpolymers synthesized.

Sample	Mn* (g/mol)	Đ†	f^v*			Mn*		
			PI	PS	PLA	PI	PS	PLA
PI-*b*-PS-*b*-PLLA	41,300	1.03	0.16	0.36	0.48	4900	13,300	23,100
PI-*b*-PS-*b*-PDLA	44,600	1.05	0.14	0.34	0.52	4900	13,300	26,400
PI-*b*-PS-*b*-PLA	42,900	1.05	0.15	0.35	0.50	4900	13,300	24,700

*Determined by ^{1}H NMR based on $\rho_{PI} = 0.83$ g/cm^3, $\rho_{PS} = 0.969$ g/cm^3, and $\rho_{PLLA} = 1.25$ g/cm^3. †Determined by GPC.

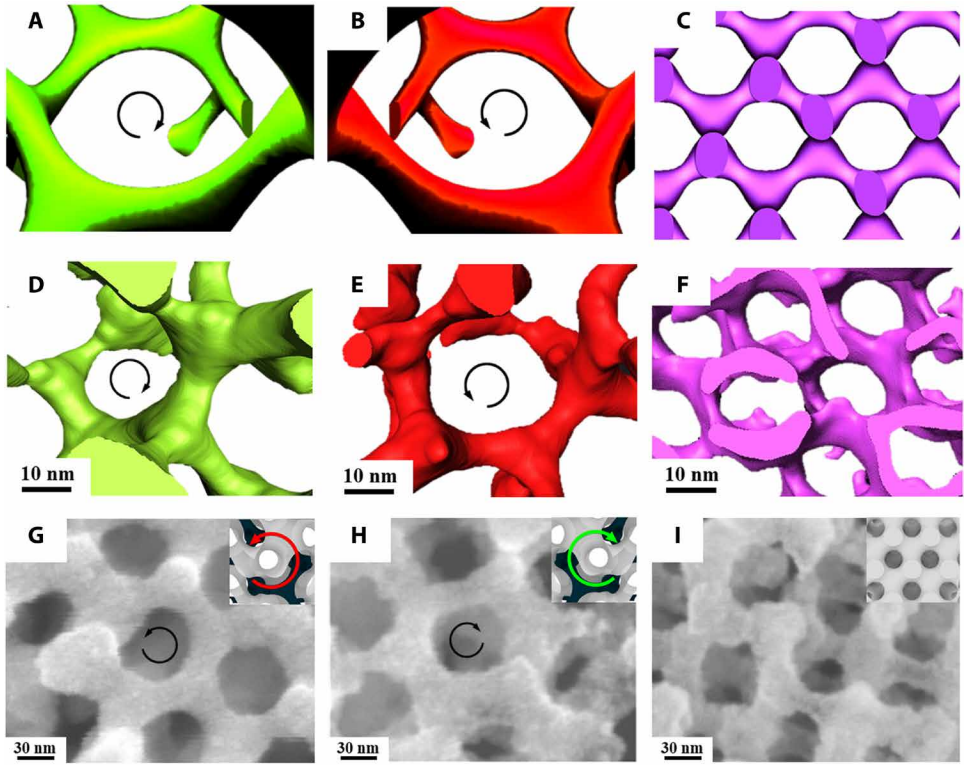

Fig. 2. 3D imaging of the PI network and SEM images of Ni network fabricated from templating of the polylactide network. (**A** to **C**) Simulated images and (**D** to **F**) 3D reconstructions from electron tomography of PI-*b*-PS-*b*-PLLA, PI-*b*-PS-*b*-PDLA, and PI-*b*-PS-*b*-PLA, respectively. Direct visualization of the right-handed [110] helical locus of the PI network in (A) and (D) and the left-handed helical locus of the PI gyroid network in (B) and (E). When an achiral PLA block is used, the structure is an achiral diamond (F). (**G** to **I**) FESEM images of the Ni network from PI-*b*-PS-*b*-PLLA, PI-*b*-PS-*b*-PDLA, and PI-*b*-PS-*b*-PLA, respectively, at which the Ni network takes on the handedness and volume fraction of the particular polylactide block that is hydrolyzed. Insets show the corresponding simulated structures with dark core struts as a visual guide. Direct visualization of the Ni gyroid network along the [111] direction demonstrates a left-handed locus in PI-*b*-PS-*b*-PLLA (G) and right-handed helical locus in PI-*b*-PS-*b*-PDLA (H).

nickel network (*33*). With the replacement of Ni for the polylactide microdomain, the SG Ni network could be directly observed by field emission scanning electron microscopy (FESEM) after removal of the template by calcination. As shown in figs. S4 (A and B), the gyroid texture of the Ni network from templating of the polylactide gyroid in the PI-*b*-PS-*b*-PLLA is readily directly visualized, providing evidence of the suggested G^A with left-handed polylactide gyroids from self-assembled chiral triblock terpolymers. The left-handed and right-handed locus of the gyroid network (Fig. 2, G and H) could be easily identified along the [111] direction for the Ni gyroid fabricated from templating of the polylactide gyroid in the PI-*b*-PS-*b*-PLLA and the PI-*b*-PS-*b*-PDLA, respectively. By contrast, an achiral Ni diamond network was found in the PI-*b*-PS-*b*-PLA sample (fig. S4C and Fig. 2I), which is consistent with the formation of a polylactide diamond in the D^A from achiral triblock terpolymer. According to the chirality analysis above, the two terpolymers, the PI-*b*-PS-*b*-PLLA and the PI-*b*-PS-*b*-PDLA, have opposite chirality for the polylactide network. Note that, in contrast to the same helical sense along [110] and [111] directions, the associated helices exhibit opposing handedness along the [100] direction (*34*). Thus, a concise and general analytic algorithm is essential to examine the chirality in the chiral gyroid network. A straightforward method for the identification of handedness determination could be developed based on the dihedral angle concept proposed by Bates and co-workers (*35*, *36*). Subsequently, a network chirality parameter based on torsion angle distribution to determine the local chirality was proposed by Grason and co-workers (*37*); the torsion angle analysis can define chirality at the smallest possible scale of the skeletal networks. To apply this analysis, we reconstructed PI gyroid network in the G^A from a single grain of self-assembled PI-*b*-PS-*b*-PLLA and PI-*b*-PS-*b*-PDLA by 3D TEM (as represented in Fig. 3A). Skeleton extraction was further adopted by mesh contraction and skeleton pruning process to acquire the connected internode networks for the examination of torsion angle (as represented in Fig. 3B and fig. S5). The torsion angle is defined as the angle between two normals ($\widehat{n_{\alpha\beta}}$ and $\widehat{n_{\beta\gamma}}$) of every three consecutive edges (r_α, r_β, and r_γ), as illustrated in Fig. 3C for right-handed (red) and left-handed (blue) SG. To systematically determine the distribution of torsion angle for the chiral network, vertex relaxation after skeleton extraction was carried out. This relaxation process can appropriately adjust the reconstructed structure from the distorted boundaries, mainly caused by the diffusion of OsO_4 staining, to its intrinsic state. The vertex relaxation is based on potential energy, which is modified from regular Keating energy (*38*) (see the Supplementary Materials for details). Note that, for a perfect gyroid network, the values for torsion angles of the reconstructed PI gyroid in the PI-PS-PLLA are at 70.5° and 250.5° while the ones in PI-*b*-PS-*b*-PDLA are −70.5° and − 250.5°, as marked by the arrows in Fig. 3 (D and E).

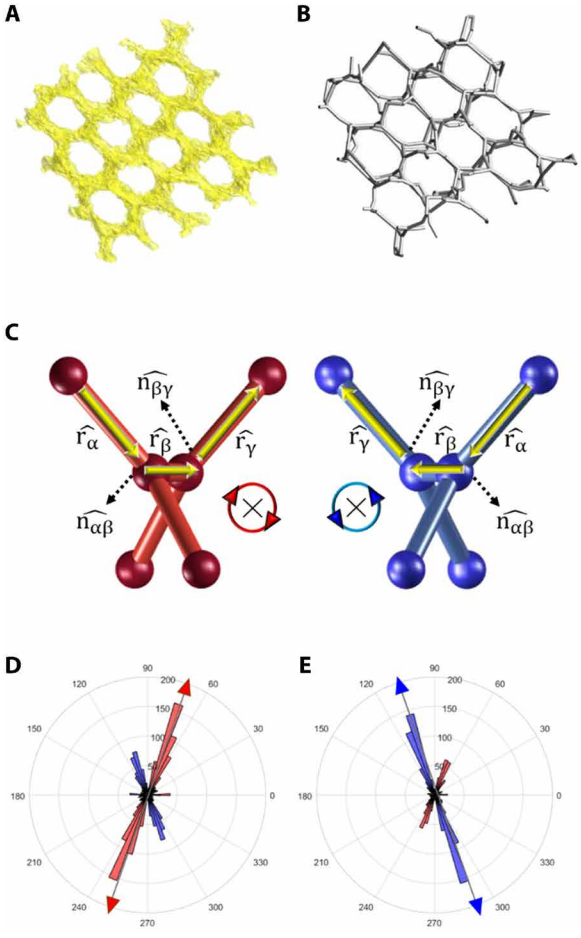

Fig. 3. Torsion angle analysis of PI gyroid in self-assembled polylactide-based triblock terpolymers from electron tomography. (**A**) Reconstructed image of the left-handed PI gyroid in the G^A of self-assembled PI-*b*-PS-*b*-PDLA. (**B**) Extracted skeleton of (A) by mesh contraction and pruning process. (**C**) The definition of torsion angle in the gyroid network for positive chirality (right-handed, red) and negative chirality (left-handed, blue), respectively. The yellow arrows indicate the vectors of three consecutive edges. The polar histogram of torsion angle distribution for PI gyroid in (**D**) PI-*b*-PS-*b*-PLLA and in (**E**) PI-*b*-PS-*b*-PDLA. The red and blue arrows indicate the torsion angles for ideal PI gyroids.

On the basis of 10-set reconstructed monograins at which more than 100 datasets per grain (more than 1000 torsion angle measurement) were acquired for each enantiomeric sample synthesized (figs. S6 and S7), as shown in Fig. 3 (D and E), the most frequent values for the torsion angle distribution of the reconstructed PI gyroid in the PI-*b*-PS-*b*-PLLA are approximately at 70° and 250° (Fig. 3D) while the ones in PI-*b*-PS-*b*-PDLA are −70° and − 250° (Fig. 3E). Notably, some of the datasets show uncertain chirality or even opposite chirality by using the analytic procedure above; note that the opposite chirality formed from the ones with preferential chirality is randomly distributed. We speculate that the ambiguity might result from several reasons: (i) various strut thicknesses due to the diffused boundaries of staining agent, (ii) missing wedge problem from 3D TEM reconstruction, (iii) structural imperfections in the original self-assembled morphology, (iv) deformation from the microtoming process, and (v) the enantiomeric impurity of samples. Accordingly, the PLLA gyroid network in the self-assembled PI-*b*-PS-*b*-PLLA can be meaningfully referred to as left-handed and the PDLA gyroid network in the PI-*b*-PS-*b*-PDLA sample can be referred to as right-handed, supporting the hypothesis that the chirality transfer occurs from monomeric unit to multichain domain network morphology in the self-assembly of the chiral triblock terpolymers.

DISCUSSION

In conclusion, two linear chiral triblock terpolymers (i.e., PI-*b*-PS-*b*-PLLA and PI-*b*-PS-*b*-PDLA) were synthesized to enable the self-assembly of networks with controlled chirality in the G^A phase. For the same composition and molecular weight, an achiral triblock terpolymer (i.e., PI-*b*-PS-*b*-PLA) was synthesized and the structure is another network phase but with no chiral character: the D^A. The molecular chirality of the chiral polylactide-based triblock terpolymers can be determined using ECD, which yields a positive Cotton effect for the PI-*b*-PS-*b*-PLLA and a negative Cotton effect for the PI-*b*-PS-*b*-PDLA. Split-type VCD spectrum with negative chirality suggests a preferred left-handed helical conformation of the PLLA chain in the PI-*b*-PS-*b*-PLLA, whereas a preferred right-handed helical conformation of the PDLA chain in the PI-*b*-PS-*b*-PDLA gives a positive chirality. Direct visualization of the PI and PLLA network in the G^A was achieved by 3D electron tomographic reconstruction and Ni network from templated synthesis. The geometric analysis on the reconstructed structures of the PI gyroid, based on measurements of the torsion angles, allows determination of chirality of the PI network. As identified by this method, PI-*b*-PS-*b*-PLLA and PI-*b*-PS-*b*-PDLA form a PI network in the G^A phase with positive chirality and negative chirality, respectively. Accordingly, controlled chirality of the polylactide gyroid can be achieved by self-assembling the chiral polylactide-based triblock terpolymer chains with the exclusive handedness of polylactide helical chain through homochiral evolution from conformation chirality to hierarchical (multichain domain) network chirality. The quantitative analysis of the correlation between the forming SG with controlled chirality and the ratio of PLLA/PDLA in the triblock terpolymer is worthy of further examination in the future. By taking advantage of the degradation characters of constituted block(s) (i.e., hydrolysis of polylactide or ozonization of polyisoprene), well-defined nanoporous polymers with a SG nanochannel can be fabricated and used for templated syntheses, such as templated atomic layer deposition, electrochemical deposition, sol-gel reaction, and electroless plating to give well-ordered nanohybrids. Such materials are promising candidates for chiroptic metamaterials such as chiral beam splitter, negative refraction, and collimation effect.

MATERIALS AND METHODS

Materials

All the manipulations and reactions were conducted under a nitrogen atmosphere using standard Schlenk line and dry-box techniques. *tert*-Butyllithium (*t*-BuLi, 1.6 M in hexane) was purchased from Sigma-Aldrich and used as received. Isoprene (purity >99.0%), styrene (purity >99.9%), and propylene oxide (purity >99.5%) were obtained from Sigma-Aldrich and distilled from CaH_2 before use. Different enantiomeric isomers of lactides, including L-lactide (purity >98.0%), D,L-lactide (purity >99.0%), and D-lactide (purity >98.0%), purchased from Sigma-Aldrich, Musashino Chemical, and Sigma-Aldrich, respectively, were purified by recrystallization in toluene before use. Stannous 2-ethylhexanoate, purchased from Sigma-Aldrich, was

diluted in toluene before use. The hydroxy-capped polyisoprene-*block*-polystyrene (PI-*b*-PS-OH) was synthesized according to literature (*39*).

General methods

^{1}H nuclear magnetic resonance (^{1}H NMR) spectra of polymers in $CDCl_3$ solution were recorded at room temperature on a Varian 500 NMR spectrometer. The polydispersity ($Đ_M$) of triblock terpolymers was examined by gel permission chromatography (GPC). The molecular weight (M_n) and the number of isoprene repeating units (N_{PI}), styrene repeating units (N_{PS}), and lactide repeating units (N_{PLA}) were determined by ^{1}H NMR. Polydispersity was calculated by using polystyrene as standard based on GPC results.

Differential scanning calorimetry (DSC) experiments were conducted by using a Perkin-Elmer DSC 7 and DSC 8000. The heat flow at constant heating rate and temperature was calibrated by using indium and cyclohexane as standards. The DSC thermograms were acquired by two procedures: One was for the measurements of low-temperature range from −80° to 0°C and the other was for the measurements of high-temperature range from 25° to 180°C. The samples were first heated at 10°C/min from 25° to 180°C for 5 min to eliminate the PLLA and PDLA crystalline residues formed during solution casting. For the high-temperature measurements, the thermally annealed samples were rapidly cooled at 150°C/min from 180° to 25°C. The thermograms were then acquired by heating at 10°C/min from 25° to 180°C for the measurements of the glass transition temperature (*T*g) of PS and PLA and the melting point (T_m) of chiral PLA. For the low-temperature measurements, the thermally annealed samples were rapidly quenched to −80°C and then heated at 10°C/min to 0°C to measure the *T*g of PI.

ECD and ultraviolet-visible absorption spectra were acquired by using a JASCO J-815 spectrometer where a quartz cell with a light path of 1.0 mm was used for the samples in the solution state. Vibrational circular dichroism (VCD) and Fourier transform infrared absorption spectra were acquired by using a JASCO FVS-6000 spectrometer where a CaF_2 cell with a light path of 50 μm was used for the samples in the solution state. The concentrations were 0.1 weight % (wt %) in AcCN for the ECD measurements and 2 wt % in dichloromethane (CH_2Cl_2) for the VCD measurements. Thin-film samples were prepared by spin casting at 500 rpm using a 2 wt % AcCN solution onto quartz substrate for the ECD measurements and a 2 wt % CH_2Cl_2 solution onto silicon wafers for the VCD measurements followed by thermal treatment at 180°C for 5 min to erase the thermal history from spin coating. After the thermal treatment, the samples were rapidly cooled at 150°C/min to 25°C for the measurements.

Bulk samples of triblock terpolymers for TEM and SAXS were first heated to 180°C for 5 min to annihilate the PDLA and PLLA crystalline residues formed during solution casting. After the thermal treatment, the samples were rapidly cooled at a rate of 150°C/min to 140°C for 1-week thermal annealing followed by rapid cooling at a rate of 150°C/min to room temperature. Thus, there should be no concern about dynamically formed deformation (*40*, *41*). Bright-field TEM images were acquired by using a JEOL JEM-2100 LaB_6 transmission electron microscope (at an accelerating voltage of 200 kV). All bulk samples were sectioned at −120°C, below the respective Tgs of constituted blocks using a Leica ultracryomicrotome to give microsections with approximately 100 nm in thickness. After the microsectioning, copper grids (100 mesh) with a polyvinyl formal film having a thickness of approximately 40 nm were used to collect the microsections. The samples were exposed to the vapor of a 4% OsO_4 aqueous solution for staining of a PI microdomain for 24 hours to give the mass-thickness contrast for TEM observations. For electron microscopy tomography (i.e., 3D TEM) experiments, the microsections on the grid were thermally annealed in the DSC furnace at 105°C for 10 s to alleviate the structural deformation during microsectioning. The thermally treated samples were stained using OsO_4 vapor for 24 hours for the required mass-thickness contrast of the PI microdomain under TEM. Fiducial gold markers with a diameter of 10 nm purchased from Polysciences Inc. were evenly dispersed on the microsections for image alignment. Then, the sample was sputter-coated with a layer of carbon to prevent the radiation damage during the TEM observation. A series of 121 TEM images were collected from −60 to +60° tilt angles along the *x* and *y* axis (dual axis) at an angular interval of 1°. Alignment of the images and 3D reconstruction were achieved by using IMOD software. Avizo 7.1.1 (Visualization Sciences Group) was then used to trim the intrinsic volume of constituted component for the reconstruction of projection images. The volume fraction in the reconstructed images after threshold is similar to the volume fraction of the constituted component measured from NMR. Consequently, visualization was accomplished by using the Avizo 7.1.1.

SAXS experiments were carried out at the synchrotron x-ray beamline 23A1 of the National Synchrotron Radiation Research Center in Hsinchu, Taiwan. Data were collected by using a Dectris Pilatus 1M-F area detector with an x-ray beam of 0.5-mm diameter and 10 keV (wavelength $\lambda = 1.24$ Å). All the experiments were conducted under ambient conditions.

Field-emission scanning electron microscopy (FESEM) observations were performed on Hitachi SU-801 using accelerating voltages of 10 kV. The samples were coated with 2 to 3 nm of platinum to eliminate the charge effect before observation; the platinum coating thickness was estimated from a calculated deposition rate and experimental deposition time.

Representative experimental procedures for the synthesis of the polylactide-based triblock terpolymers

A series of PI-*b*-PS-*b*-PLA, PI-*b*-PS-*b*-PLLA, and PI-*b*-PS-*b*-PDLA samples were synthesized via living anionic polymerization [for syntheses of hydroxyl-capped polyisoprene-*block*-polystyrene (PI-*b*-PS-OH) as a precursor for macroinitiator] and controlled ring-opening polymerization reactions in sequence (scheme S1). The PI-*b*-PS-OH was synthesized according to literature (*39*).

A 100-ml Schlenk flask was sequentially charged with freshly prepared PI-*b*-PS-OH (0.33 mM) in toluene and 0.33 mmol of stannous 2-ethylhexanoate in a dry box. The resultant solution was stirred at 80°C for 0.5 hours for the generation of the macroinitiator. After the formation of the macroinitiator, the resultant solution was charged with 0.80 g of L-lactide (5.6 mmol) and then heated to 120°C to initiate the copolymerization of PLLA block with the PI-*b*-PS-OH. The controlled living copolymerization of L-lactide was conducted at 120°C for 3 hours. The copolymerization reaction was terminated by introducing 50 ml of methanol, giving the precipitation of the reaction product. The resultant slurry was filtered and dried under vacuum to give PI-*b*-PS-*b*-PLLA [M_n = 41,300 g/mol, $Đ_M$ = 1.03 by GPC (in THF at 40°C)]. Similar synthetic routes were carried out for the syntheses of PI-*b*-PS-*b*-PLLD and PI-*b*-PS-*b*-PLA.

Torsion angle analysis

To examine the chirality of reconstructed PI gyroids from PI-*b*-PS-*b*-PDLA and PI-*b*-PS-*b*-PLLA, the skeletons that represent the

structural characteristics of the PI gyroids were extracted from the 3D images. Figure S5 is a schematic diagram that illustrates the process flow of skeleton extraction. Initially, the raw data were obtained from the 3D image by Avizo, as shown in fig. S5A. A relatively noise-insensitive thinning algorithm was developed to get the skeleton. In the thinning process, the surface boundary is peeled off iteratively by a mesh processing algorithm (fig. S5B), implemented based on constrained Laplacian geometry smoothing along with mesh simplification (*42*). After thinning, the skeletons are extracted, where three-arm junction nodes can be identified. The network was reconstructed by connecting those three-arm nodes based on the original connected trajectory (fig. S5C), followed by a pruning process to remove struts outside the trajectory (fig. S5D). Then, struts nearby the boundaries were removed to eliminate the boundary effects (fig. S5E). After these procedures, the structural skeletons with identified nodes could be obtained (fig. S5F) for structural analysis.

It should be noted that there might be imperfection of the raw data of PI gyroid for reconstruction resulting from sample preparation for imaging. Owing to the low Tg of PI, the microsectioning may give rise to network deformation. Most notoriously, the OsO4 staining for the enhancement of the mass-thickness contrast will result in diffused boundaries of the PI network with the PS matrix, leading to distortion of the reconstructed framework of strut from the intrinsic network. Consequently, the reconstructed skeleton might encounter uneven shrinkage of struts or even disconnection after reconstruction. To examine the chirality of reconstructed network, a vertex relaxation method was thus adopted. The vertex relaxation is a process of optimizing the location of vertex, where the structure is relaxed to minimize a modified Keating potential function, described by (*38*, *43*)

$$E = \alpha f_1(\{d\}) + \beta f_2(\{\theta\}) + \gamma f_3(\{\phi\}) + \delta f_4(\{\chi\}) \quad (1)$$

where the function f_1 accounts for the deviation of bond length d from the mean bond length of the skeleton and f_2 accounts for the deviation of bond angle θ from 120° as in an ideal SG network. The functions f_3 and f_4 evaluate the deviation of the dihedral angle and skew angle from an ideal SG network, described as (*38*)

$$f_3 = \Sigma_i \Sigma_j (\,|\,\hat{n}(i_1,i_2)\cdot\hat{n}(j_1,j_2)\,|\;\; -1/3)^2 \quad (2)$$

$$f_4 = \Sigma_i \Sigma_j (\hat{r}(i,j)\cdot\hat{n}(i_1,i_2))^2 + (\hat{r}(i,j)\cdot\hat{n}(j_1,j_2))^2 \quad (3)$$

where $\hat{r}(i,j)$ represents the unit vector from i to j and $\hat{n}(i_1,i_2)$ represents the unit normal to the plane containing the vectors $\hat{r}(i,i_1)$ and $\hat{r}(i,i_2)$ (fig. S8). There are two possible dihedral angles of ideal SG skeleton, which are $\arccos(\pm\frac{1}{3}) = 70.5°$ and 109.5° for right-handed SG and −70.5° and −109.5° for left-handed SG. If the vertex is unable to be calculated in f_3 and f_4 because of the inevitable disconnection defects, the relaxation base of the vertex will be reorganized to be f_1 and f_2 only. Note that the connective order of struts remains the same during the relaxation process. In each iteration, a vertex position is optimized by using the MATLAB optimizing toolbox to lower the modified Keating energy, and a global relaxation is processed after 100 local relaxations to avoid local minima.

SG is among the most interesting network phases that exhibit inherent chirality. As described in the Results section of torsion angle analysis, an effective method for the determination of chirality was developed based on torsion angle analysis by Grason and co-workers (*37*). As shown in fig. S8B (dog-bone–like ideal SG skeleton), the torsion angle θ_t is defined by three consecutive struts as

$$\sin(\theta_t) = (\widehat{n_{\alpha\beta}} \times \widehat{n_{\beta\gamma}})\cdot\widehat{r_\beta} \quad (4)$$

$$\cos(\theta_t) = \widehat{n_{\alpha\beta}}\cdot\widehat{n_{\alpha\beta}} \quad (5)$$

As a result, an ideal SG network yields torsion angles of 70.5° or 250.5° for positive chirality and −70.5° (109.5°) or −250.5 (289.5°) for negative chirality.

For a systematic examination of chirality, 20 sets of reconstruction images with a size of 3 × 3 × 1.5 unit cells from the PI-*b*-PS-*b*-PLLA and PI-*b*-PS-*b*-PDLA samples (each with ten sets) were acquired from the OsO_4-stained PI microsections. The reconstruction images were acquired from different batches of samples. It is noted that variations of samples during preparation and limited construction frame size around 8 nm may result in some reconstruction defects. As described in the Results section of electron tomography, the acquired tomographic images are representative of the monograins with exclusive chirality as examined. The raw data and the corresponding thinning results were uploaded on the website (https://drive.google.com/open?id=1VpKuXPA_NVzUYXau5gJZ1q966sK_2BwF).

The analysis results based on the aforementioned vertex relaxation method are shown in figs. S6 and S7. For the analytic measurement, there are 20 polar histograms acquired from the raw data. For the PI-*b*-PS-*b*-PDLA samples (fig. S6), 9 of 10 sets show consistent results with negative chirality with torsion angles of 70.5° or 250.5° (109.5° or 289.5°), while one set shows less prominent chiral bias. For the PI-*b*-PS-*b*-PDLA samples (fig. S7), six sets yield consistent positive chirality, whereas two sets are with negative chirality and two show weaker chiral bias.

Templated synthesis

After rapid cooling from microphase-separated ordered melt, the polylactide segments in the polylactide-based triblock terpolymers were degenerated by hydrolysis using a sodium hydroxide solution of methanol/water (0.5 M) for 7 days. After hydrolysis, nanoporous polymers with SG- or SD-structured nanochannels can be prepared and used as templates for following electroless plating reaction. The nanoporous templates were soaked in an activating solution composed of HCl (1 N, 5 ml), ethanol (45 ml), and $PdCl_2$ (0.05 g) after stirring at room temperature for 1 hour. The pore-filled templates were immersed into a freshly prepared Ni bath consisting of 0.2 g of nickel chloride ($NiCl_2{\cdot}6H_2O$) dissolved in a solution of ethanol (5 ml), distilled water (20 ml), ammonia (2 ml), and hydrazinium hydroxide (85%, 2 ml) at room temperature for fabrication of aimed nanohybrids. To obtain the nanoporous SG- and SD-structured Ni, the polymeric materials in the fabricated nanohybrids were degenerated by thermal degradation at 450°C for 12 hours.

Simulation for 3D networks

To simulate the morphologies with the same volume fraction as the reconstructed results for SG and SD, the surfaces were trigonometrically calculated by using the following nodal approximation equations

$$\sin(x)\cos(y) + \sin(y)\cos(z) + \sin(z)\cos(x) = t \quad (6)$$

$$\sin(x)\sin(y)\sin(z)+\sin(x)\cos(y)\cos(z)+\cos(x)\sin(y)\cos(z)+\cos(x)\cos(y)\sin(z)=t \quad (7)$$

where Eq. 6 was used for the SG surface and Eq. 7 was used for the SD surface. The threshold parameter "t" in the equations determines volume fraction embedded by level surface. For SG and SD with the volume fraction of 0.15, the values of t equal to 1.057 and 0.842, respectively.

SUPPLEMENTARY MATERIALS

Supplementary material for this article is available at http://advances.sciencemag.org/cgi/content/full/6/42/eabc3644/DC1

REFERENCES AND NOTES

1. V. Luzzati, P. Spegt, Polymorphism of lipids. *Nature* **215**, 701–704 (1967).
2. S. Tretyakov, I. Nefedov, A. Sihvola, S. Maslovski, C. Simovski, Waves and energy in chiral nihility. *J. Electromagn. Waves Appl.* **17**, 695–706 (2003).
3. J. Pendry, A chiral route to negative refraction. *Science* **306**, 1353–1355 (2004).
4. C. Monzon, D. Forester, Negative refraction and focusing of circularly polarized waves in optically active media. *Phys. Rev. Lett.* **95**, 123904 (2005).
5. A. Papakostas, A. Potts, D. M. Bagnall, S. L. Prosvirnin, H. J. Coles, N. I. Zheludev, Optical manifestations of planar chirality. *Phys. Rev. Lett.* **90**, 107404 (2003).
6. G. Horváth, G. Horváth, D. Varju, G. Horváth, *Polarized Light in Animal Vision: Polarization Patterns in Nature* (Springer Science & Business Media, 2004).
7. M. D. Turner, M. Saba, Q. Zhang, B. P. Cumming, G. E. Schröder-Turk, M. Gu, Miniature chiral beamsplitter based on gyroid photonic crystals. *Nat. Photonics* **7**, 801–805 (2013).
8. S. S. Oh, A. Demetriadou, S. Wuestner, O. Hess, On the origin of chirality in nanoplasmonic gyroid metamaterials. *Adv. Mater.* **25**, 612–617 (2013).
9. S. Salvatore, A. Demetriadou, S. Vignolini, S. S. Oh, S. Wuestner, N. A. Yufa, M. Stefik, U. Wiesner, J. J. Baumberg, O. Hess, U. Steiner, Tunable 3D extended self-assembled gold metamaterials with enhanced light transmission. *Adv. Mater.* **25**, 2713–2716 (2013).
10. J. A. Dolan, B. D. Wilts, S. Vignolini, J. J. Baumberg, U. Steiner, T. D. Wilkinson, Optical properties of gyroid structured materials: From photonic crystals to metamaterials. *Adv. Opt. Mater.* **3**, 12–32 (2015).
11. D. A. Hajduk, P. E. Harper, S. M. Gruner, C. C. Honeker, G. Kim, E. L. Thomas, L. J. Fetters, The gyroid: A new equilibrium morphology in weakly segregated diblock copolymers. *Macromolecules* **27**, 4063–4075 (1994).
12. M. F. Schulz, F. S. Bates, K. Almdal, K. Mortensen, Epitaxial relationship for hexagonal-to-cubic phase transition in a book copolymer mixture. *Phys. Rev. Lett.* **73**, 86–89 (1994).
13. M. W. Matsen, M. Schick, Stable and unstable phases of a diblock copolymer melt. *Phys. Rev. Lett.* **72**, 2660–2663 (1994).
14. P. Mariani, V. Luzzati, H. Delacroix, Cubic phases of lipid-containing systems: Structure analysis and biological implications. *J. Mol. Biol.* **204**, 165–189 (1988).
15. K. Fontell, Cubic phases in surfactant and surfactant-like lipid systems. *Colloid Polym. Sci.* **268**, 264–285 (1990).
16. G. P. Sorenson, K. L. Coppage, M. K. Mahanthappa, Unusually stable aqueous lyotropic gyroid phases from gemini dicarboxylate surfactants. *J. Am. Chem. Soc.* **133**, 14928–14931 (2011).
17. V. Saranathan, C. O. Osuji, S. G. J. Mochrie, H. Noh, S. Narayanan, A. Sandy, E. R. Dufresne, R. O. Prum, Structure, function, and self-assembly of single network gyroid (I4132) photonic crystals in butterfly wing scales. *Proc. Natl. Acad. Sci. U.S.A.* **107**, 11676–11681 (2010).
18. G. E. Schröder-Turk, S. Wickham, H. Averdunk, F. Brink, J. D. Fitz Gerald, L. Poladian, M. C. J. Large, S. T. Hyde, The chiral structure of porous chitin within the wing-scales of *Callophrys rubi*. *J. Struct. Biol.* **174**, 290–295 (2011).
19. B. Winter, B. Butz, C. Dieker, G. E. Schröder-Turk, K. Mecke, E. Spiecker, Coexistence of both gyroid chiralities in individual butterfly wing scales of *Callophrys rubi*. *Proc. Natl. Acad. Sci. U.S.A.* **112**, 12911–12916 (2015).
20. T. H. Epps, E. W. Cochran, T. S. Bailey, R. S. Waletzko, C. M. Hardy, F. S. Bates, Ordered network phases in linear poly (isoprene-b-styrene-b-ethylene oxide) triblock copolymers. *Macromolecules* **37**, 8325–8341 (2004).
21. S. Vignolini, N. A. Yufa, P. S. Cunha, S. Guldin, I. Rushkin, M. Stefik, K. Hur, U. Wiesner, J. J. Baumberg, U. Steiner, A 3D optical metamaterial made by self-assembly. *Adv. Mater.* **24**, OP23–OP27 (2012).
22. R.-M. Ho, Y.-W. Chiang, C.-C. Tsai, C.-C. Lin, B.-T. Ko, B.-H. Huang, Three-dimensionally packed nanohelical phase in chiral block copolymers. *J. Am. Chem. Soc.* **126**, 2704–2705 (2004).
23. R.-M. Ho, Y.-W. Chiang, C.-K. Chen, H.-W. Wang, H. Hasegawa, S. Akasaka, E. L. Thomas, C. Burger, B. S. Hsiao, Block copolymers with a twist. *J. Am. Chem. Soc.* **131**, 18533–18542 (2009).
24. R.-M. Ho, Y.-W. Chiang, S.-C. Lin, C.-K. Chen, Helical architectures from self-assembly of chiral polymers and block copolymers. *Prog. Polym. Sci.* **36**, 376–453 (2011).
25. R.-M. Ho, M.-C. Li, S.-C. Lin, H.-F. Wang, Y.-D. Lee, H. Hasegawa, E. L. Thomas, Transfer of chirality from molecule to phase in self-assembled chiral block copolymers. *J. Am. Chem. Soc.* **134**, 10974–10986 (2012).
26. T. Wen, H.-F. Wang, M.-C. Li, R.-M. Ho, Homochiral evolution in self-assembled chiral polymers and block copolymers. *Acc. Chem. Res.* **50**, 1011–1021 (2017).
27. H.-F. Wang, K.-C. Yang, W.-C. Hsu, J.-Y. Lee, J.-T. Hsu, G. M. Grason, E. L. Thomas, J.-C. Tsai, R.-M. Ho, Generalizing the effects of chirality on block copolymer assembly. *Proc. Natl. Acad. Sci. U.S.A.* **116**, 4080–4089 (2019).
28. T. H. Epps, F. S. Bates, Effect of molecular weight on network formation in linear ABC triblock copolymers. *Macromolecules* **39**, 2676–2682 (2006).
29. Y. Asai, J. Suzuki, Y. Aoyama, H. Nishioka, A. Takano, Y. Matsushita, Tricontinuous double diamond network structure from binary blends of ABC triblock terpolymers. *Macromolecules* **50**, 5402–5411 (2017).
30. E. Yashima, K. Maeda, Chirality-responsive helical polymers. *Macromolecules* **41**, 3–12 (2008).
31. E. Schwartz, S. R. Domingos, A. Vdovin, M. Koepf, W. J. Buma, J. J. L. M. Cornelissen, A. E. Rowan, R. J. M. Nolte, S. Woutersen, Direct access to polyisocyanide screw sense using vibrational circular dichroism. *Macromolecules* **43**, 7931–7935 (2010).
32. K. Nakanishi, N. Berova, R. Woody, *Circular Dichroism: Principles and Applications* (VCh, 1994).
33. H.-Y. Hsueh, Y.-C. Huang, R.-M. Ho, C.-H. Lai, T. Makida, H. Hasegawa, Nanoporous gyroid nickel from block copolymer templates via electroless plating. *Adv. Mater.* **23**, 3041–3046 (2011).
34. M. Saba, B. D. Wilts, J. Hielscher, G. E. Schröder-Turk, Absence of circular polarisation in reflections of butterfly wing scales with chiral gyroid structure. *Mater. Today* **1**, 193–208 (2014).
35. T. S. Bailey, C. M. Hardy, T. H. Epps, F. S. Bates, A noncubic triply periodic network morphology in poly (isoprene-*b*-styrene-*b*-ethylene oxide) triblock copolymers. *Macromolecules* **35**, 7007–7017 (2002).
36. Z. Li, K. Hur, H. Sai, T. Higuchi, A. Takahara, H. Jinnai, S. M. Gruner, U. Wiesner, Linking experiment and theory for three-dimensional networked binary metal nanoparticle–triblock terpolymer superstructures. *Nat. Commun.* **5**, 3247 (2014).
37. I. Prasad, H. Jinnai, R.-M. Ho, E. L. Thomas, G. M. Grason, Anatomy of triply-periodic network assemblies: Characterizing skeletal and inter-domain surface geometry of block copolymer gyroids. *Soft Matter* **14**, 3612–3623 (2018).
38. S. R. Sellers, W. Man, S. Sahba, M. Florescu, Local self-uniformity in photonic networks. *Nat. Commun.* **8**, 14439 (2017).
39. C. D. Cowman, E. Padgett, K. W. Tan, R. Hovden, Y. Gu, N. Andrejevic, D. Muller, G. W. Coates, U. Wiesner, Multicomponent nanomaterials with complex networked architectures from orthogonal degradation and binary metal backfilling in ABC triblock terpolymers. *J. Am. Chem. Soc.* **137**, 6026–6033 (2015).
40. G. E. S. Toombes, A. C. Finnefrock, M. W. Tate, R. Ulrich, U. Wiesner, S. M. Gruner, A re-evaluation of the morphology of a bicontinuous block copolymer–ceramic material. *Macromolecules* **40**, 8974–8982 (2007).
41. X. Feng, C. J. Burke, M. Zhuo, H. Guo, K. Yang, A. Reddy, I. Prasad, R.-M. Ho, A. Avgeropoulos, G. M. Grason, E. L. Thomas, Seeing mesoatomic distortions in soft-matter crystals of a double-gyroid block copolymer. *Nature* **575**, 175–179 (2019).
42. O. K.-C. Au, C.-L. Tai, H.-K. Chu, D. Cohen-Or, T.-Y. Lee, *ACM Transactions on Graphics (TOG)* (ACM, 2008), vol. 27, 44 pp.
43. P. N. Keating, Effect of invariance requirements on the elastic strain energy of crystals with application to the diamond structure. *Phys. Rev.* **145**, 637–645 (1966).

Acknowledgments: Helpful discussion with G. M. Grason is highly appreciated. **Funding:** We thank the Ministry of Science and Technology (MOST), Taiwan, for financially supporting this research under contract no. MOST 107-2221-E-007-030-MY3 and the Air Force Office of Scientific Research (US) under Asian Office of Aerospace Research and Development Award 18IOA088. This work was partially supported by JSPS KAKENHI, Japan (grant nos. 16H02288 and 19H00905). This work was also partially supported by JST CREST (grant no. JPMJCR1993), Japan. **Author contributions:** R.-M.H. designed and directed the project, and E.L.T. provided the suggestions and comments on the project. H.-F.W. and P.-T.C. performed the experiments of the self-assembly of chiral triblock terpolymers and 3D TEM experiments of the SG and SD structures. R.-M.H., J.-Y.L., and J.-C.T. designed, synthesized, and characterized the chiral triblock terpolymers. R.-M.H. and H.-F.W. developed the methodology for the examination of chirality transfer from molecule to hierarchical in the self-assembly of chiral triblock

terpolymers. H.J. provided help and suggestions on the 3D TEM experiments. I.P. initiated the methodology for the torsion angle analysis. C.-Y.Y., Z.-H.X., and Y.-C.H. developed the methodology for the torsion angle analysis. R.-M.H., E.L.T., H.-F.W., P.-T.C., J.-Y.L., J.-C.T., C.-Y.Y., and Y.-C.H. wrote the manuscript. All authors discussed the results and commented on the manuscript. **Competing interests:** The authors declare that they have no competing interests. **Data and materials availability:** All data needed to evaluate the conclusions in the paper are present in the paper and/or the Supplementary Materials. Additional data related to this paper may be requested from the authors.

Submitted 23 April 2020
Accepted 28 August 2020
Published 14 October 2020
10.1126/sciadv.abc3644

Citation: H.-F. Wang, P.-T. Chiu, C.-Y. Yang, Z.-H. Xie, Y.-C. Hung, J.-Y. Lee, J.-C. Tsai, I. Prasad, H. Jinnai, E. L. Thomas, R.-M. Ho, Networks with controlled chirality via self-assembly of chiral triblock terpolymers. *Sci. Adv.* **6**, eabc3644 (2020).

Science Advances

Networks with controlled chirality via self-assembly of chiral triblock terpolymers

Hsiao-Fang Wang, Po-Ting Chiu, Chih-Ying Yang, Zhi-Hong Xie, Yu-Chueh Hung, Jing-Yu Lee, Jing-Cherng Tsai, Ishan Prasad, Hiroshi Jinnai, Edwin L. Thomas and Rong-Ming Ho

Sci Adv **6** (42), eabc3644.
DOI: 10.1126/sciadv.abc3644

Science Advances (ISSN 2375-2548) is published by the American Association for the Advancement of Science, 1200 New York Avenue NW, Washington, DC 20005. The title *Science Advances* is a registered trademark of AAAS.